Bulletin of the Seismological Society of America, Vol. 97, No. 4, pp. 1355–1363, August 2007, doi: 10.1785/0120060158

Short Note

Lateral Variation in the Sedimentary Structure of West Bohai Bay Basin Inferred from *P*-Multiple Receiver Functions

by Juan Li, Baofeng Tian, Weimin Wang, Lianfeng Zhao, and Zhenxing Yao

Abstract The widely distributed Cenozoic sediments in the Bohai Bay Basin give rise to noticeable modification of broadband teleseismic *P* waveforms. At one station in the west Bohai Bay Basin, the observed amplitude of tangential *P*-receiver functions is significantly above the noise level, and sedimentary reverberations (e.g., the *P*-type wave *PpPp*) remain one of the most prominent features in both the radial and tangential components. To investigate the lateral heterogeneity structure under this site, a 3D raytracing technique is used to compute the teleseismic *P*-wave response, and a fast simulated annealing algorithm is applied to the simultaneous inversion of radial receiver functions for different backazimuths. An upper crustal structure consisting of shallow dipping sedimentary layers with low seismic velocities and large Poisson's ratios is proposed to interpret the observed seismic data. The west-dipping interfaces we obtained are consistent with the north-northeast–south-southwest surface geology in North China, and Tertiary extensional fault structures may be responsible for the formation of dipping sedimentary layers.

Introduction

The Bohai Bay Basin, a major continental petroliferous basin, is located in the east part of North China Craton (NCC). The North China cratonic nucleus consists of Archaean and Proterozoic granites and metamorphic basement, cropping out the west and north of the Bohai Bay Basin. During the Mesozoic and Cenozoic eras, the NCC underwent several distinct phases of rifting and subsidence (Ye *et al.*, 1985), resulting in a large-scale thick Tertiary and Quaternary subaerial deposits cover. The subduction rollback of the Pacific plate relative to the eastern margin of Asia is probably the most important tectonic control on the extension of NCC (e.g., Allen *et al.*, 1997; Lu *et al.*, 1997).

Bounded by the Taihang Mountain to the west. Yan Mountain to the north, Jiaoliao Uplift to the east, and Luxi to the south, the rhombic shape of Bohai Bay Basin (Fig. 1) was developed on the pre-Tertiary strata. Tertiary strata rest unconformably on a variety of older prerift strata and are covered conformably or disconformably by Quaternary sediments, and the succession is typically 4000–7000 m thick (Allen *et al.*, 1997). Considering the Cenozoic rift history of the basin, a two-stage evolution model has been popularly accepted, which includes Paleogene rifting and differential subsidence and Neogene postrift thermal subsidence (e.g., Ye *et al.*, 1985; Yang and Xu, 2004). Tertiary syn-rift strata form the major hydrocarbon source and reservoir rocks of the basin (Allen *et al.*, 1997).

The basic understanding of Bohai Bay Basin comes from surface geological surveys, well-logging data, and seismic reflection/refraction profilings, concentrating mainly on the petroleum exploration and complex tectonic evolution history of the basin (e.g., Ren *et al.*, 2002; Li, 2004; Yang and Xu, 2004). With the increase of digital broadband seismic records, some geophysical investigations have been made to image the detailed upper mantle structure under the basin (e.g., Zhao and Zheng, 2005; Zheng *et al.*, 2005; Zhao *et al.*, 2006). Initial results show that thick layers of widely distributed Cenozoic sediments are one of the most particular features in the Bohai Bay Basin, which can give rise to noticeable modification of broadband waveforms due to the extreme velocity contrasts existing at the bottom of the structures.

The receiver function technique has been widely applied for determining gross- or fine-scale (i.e., 1- to 2-km-thick layers) crust and mantle structure under arrays of broadband stations (e.g., Burdick and Langston, 1977; Owens and Crosson, 1988; Ammon *et al.*, 1990; Zhu and Kanamori, 2000). At sites where shallow complexities (e.g., anisotropy, dipping interfaces) are found, however, care must be taken in interpretation of receiver functions for deeper structure (Owens and Crosson, 1988; Zhang and Langston, 1995; Zhu *et al.*, 1995; Anandakrishnan and Winberry, 2004). Using the teleseismic receiver functions, this article examines a

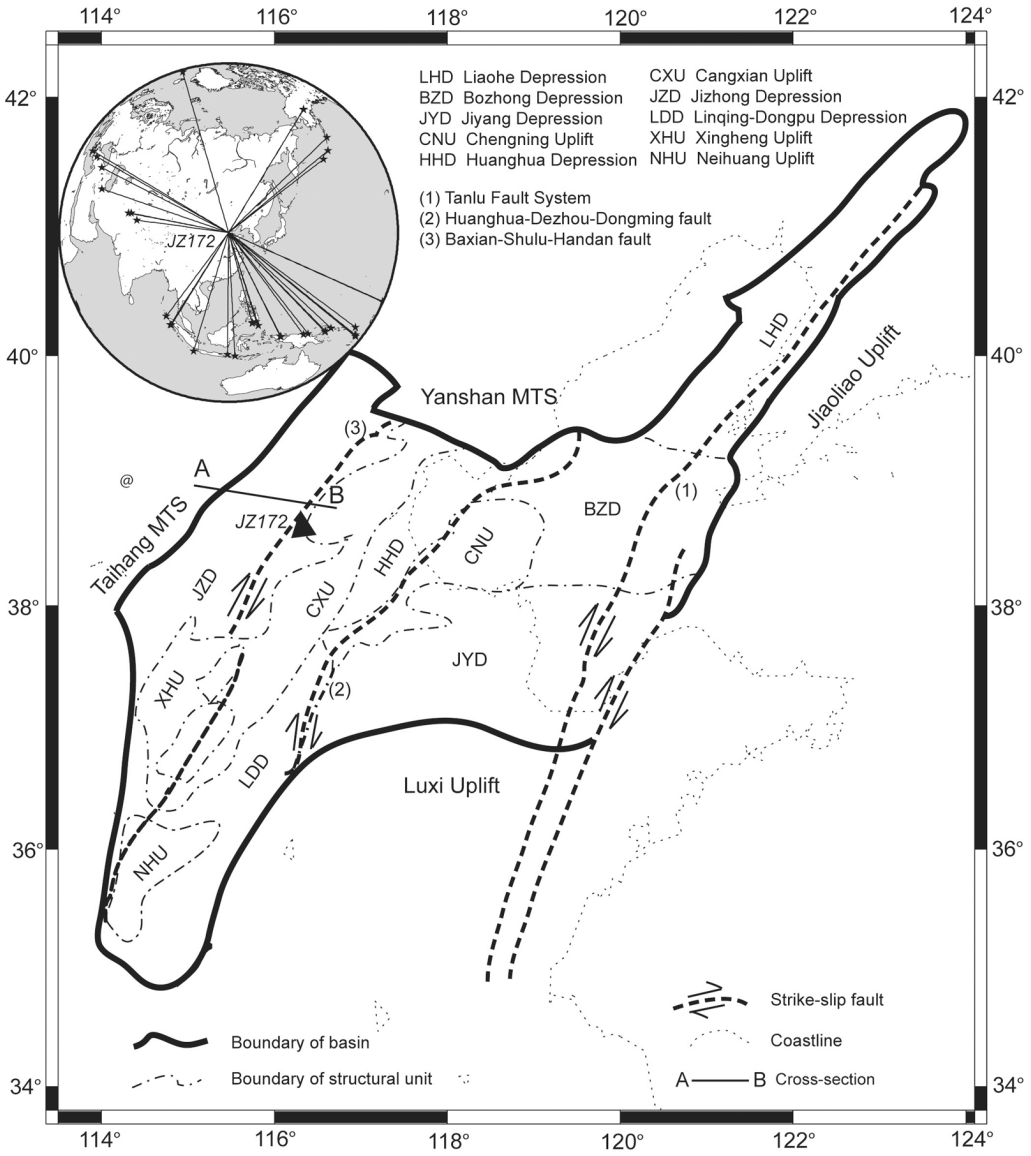

Figure 1. Geological sketch map of the Bohai Bay Basin and Cenozoic structural units (modified from Zhao and Windley, 1990; Lu *et al.*, 1997). The upper-left inset shows the locations of 37 teleseismic events collected at station JZ172.

case in the west Bohai Bay Basin, where the seismic data cannot be explained with a simple homogeneous horizontally layered earth model. Large-amplitude tangential receiver functions are observed under station JZ172 (Fig. 1). The prominent *P*-type sedimentary reverberations are identified and the amplitude variation of multiple phases in the radial receiver functions is analyzed to obtain the laterally heterogeneous structure under the station. An upper crustal structure consisting of shallow west-dipping sedimentary layers with low seismic velocities is proposed to interpret the observed seismic data, the modeling results and geological implications are discussed in the following sections.

Dipping Sedimentary Layer Effects on Receiver Functions

The most common case of lateral heterogeneity is planar dipping layers. Previous work has focused mainly on the amplitude variation of the converted *Ps* phase generated at dipping interfaces (e.g., Cassidy, 1992; Zhu *et al.*, 1995). Considering the observed large amplitude of multiple phases in our case, however, a numerical experiment is made to demonstrate the effect of a dipping sedimentary layer on receiver functions. In Figure 2c, the synthetic radial and tangential receiver functions for a model with a 2-km-thick sedimentary layer dipping 15° to the west are shown. We cal-

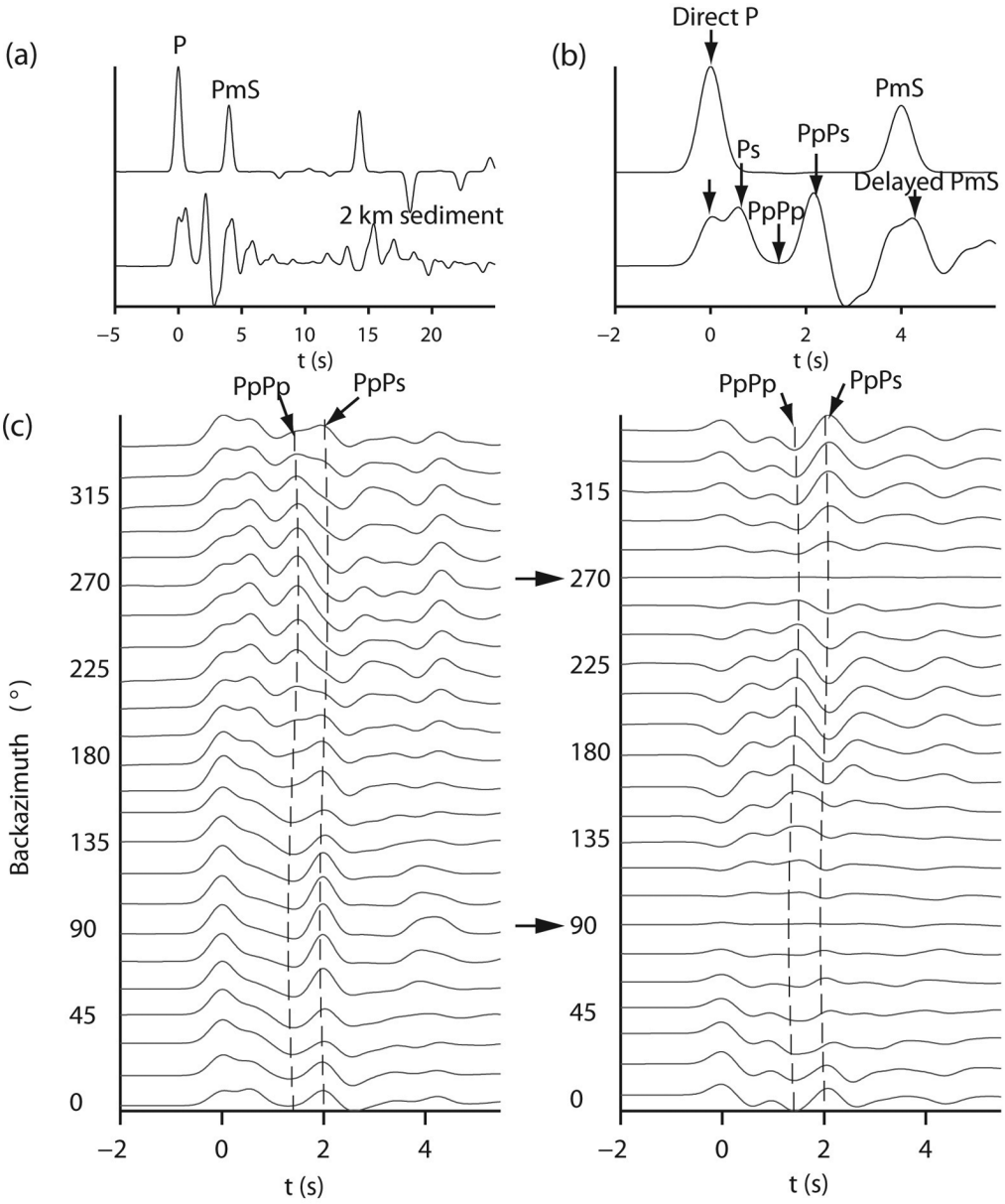

Figure 2. (a) Synthetic receiver functions for a one-layer crust model (upper curve), two-layer model (2-km-thick sedimentary layer over crust) (lower curve). (b) Enlarged view of the first 6 sec of receiver functions for the same cases as in (a). (c) Synthetic receiver functions for a model with a sedimentary layer dipping 15° to the west; left and right panels are for radial and tangential components, respectively (V_p = 2.50 km/sec, V_s = 1.44 km/sec above the dipping interface, V_p = 5.10 km/sec, V_s = 3.00 km/sec below, and the Moho is at depth of 28 km with V_p = 7.8 km/sec). The two arrows point to where the polarity of the direct *P* wave changes in the tangential component.

culated the synthetic receiver functions at backazimuth intervals of 15° according to a 3D raytracing method of Langston (1977). The ray parameters are fixed at 0.068 sec/km. For comparison, the receiver functions for a horizontally layered model are also calculated (Fig. 2a), and Figure 2b is an enlarged view of the first several seconds part of the radial receiver function.

It can be seen that the addition of a sedimentary layer obscures all the phases up to the Moho multiples and the shape of the first 5 sec of receiver functions is mainly controlled by the sedimentary layer. Despite the already known fact that tangential receiver functions form mirror images across a line parallel to the dip direction, in Figure 2c, another obvious feature can be detected. The *P*-multiple phase

PpPp, which cannot be observed in a horizontally layered case, not the *Pms*-converted phase, is most prominent with large variations of amplitude immediately following the direct *P* wave. For example, it shows a positive polarity when the ray arrives in an updip direction and turns negative for downdip arrivals in the radial receiver functions.

With the changing of dip angle, the amplitude of multiple phase *PpPp* also varies systematically. In Figure 3, we show the variation of the radial and tangential amplitude of *PpPp* with backazimuth quantitatively for the same model but with three different dip angles. The symmetric or antisymmetric amplitude variation of the *PpPp* phase can also be identified clearly in Figure 3a. When the dip angle is relatively small, the variation of *PpPp* displays a simple mode both in the radial and tangential receiver functions. However, with increasing dip angle, for example, a dip angle of 15°, the amplitude of *PpPp* changes rapidly around the dip direction, introducing a more complex amplitude variation mode.

To investigate the trade-off between dip angle and velocity contrast across the interface (Owens and Crosson, 1988), we calculate the maximum amplitude of *PpPp* with backazimuth at different dip angles. The *P* velocity V_p of the sedimentary layer is fixed at 2.5 km/sec, and the V_p/V_s ratio is changed from 1.73 to 2.73. Figure 3b is the variation of maximum radial and tangential amplitude with $\Delta(V_p/V_s)$ ($\Delta(V_p/V_s) = V_p/V_s - 1.73$) in the sedimentary layer. The dip angle controls the shape and amplitude variation with backazimuth and also the maximum radial and tangential amplitude. The value of $\Delta(V_p/V_s)$, or the velocity difference across the interface, however, contributes mainly to the maximum amplitude, which is more sensitive to the maximum amplitude variation than the dip angle both in the radial and tangential receiver functions.

Therefore, it is possible to determine the dip and strike directions of the dipping sediments by examining a backazimuthal profile of receiver functions. Especially when multiple phases (e.g., *PpPp*, which closely follows the direct *P* wave) could be detected according to the preceding characteristics, the information provided by variation of polarity, amplitude, and arrival time of multiple phases could be used to constrain the sedimentary structure in detail.

Data Analysis and Results

In recent years, hundreds of portable seismic stations were deployed in an experiment called the Northern China Interior Structure Project (NCISP), and abundant high-quality digital data were collected at densely distributed stations. Excellent backazimuthal coverage of records from NCISP enables us to study the lateral variation in the sedimentary and upper crustal structure using the teleseismic receiver function waveforms. Here, we focus our attention on station JZ172 (38.60° N, 116.18° E) located in the east

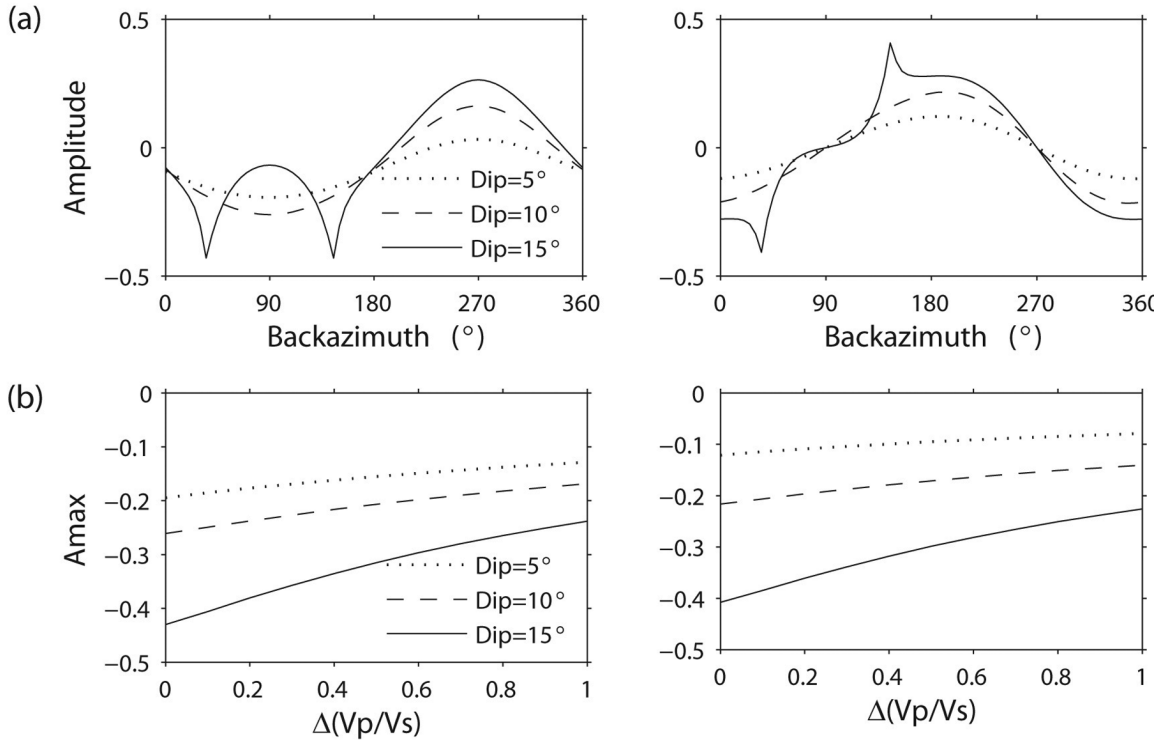

Figure 3. (a) Amplitude variation of the *PpPp* phase with backazimuth at different dip angles. (b) Variation of the maximum amplitude of *PpPp* with $\Delta(V_p/V_s)$ of the sedimentary layer at different dip angles. Left and right panels are for radial and tangential components, respectively.

edge of Jizhong depression (Fig. 1), for the initial receiver function analysis shows that the amplitude of tangential receiver functions is large and significantly above the seismic noise level, which is an obvious indicator of strong lateral heterogeneity beneath the site.

Thirty-seven events with high signal-to-noise ratio are selected for station JZ172 with magnitude >5.5 and distance range from 30° to 90° (Fig. 1). The *P* arrivals are first measured by cross-correlating vertical components of waveforms of each earthquake, which could be used as a data quality check to identify instrument problems such as polarity reversal. The three-component recordings are cut with a time window of 120-sec length beginning 20 sec before the direct *P* arrival. Then the receiver functions are obtained using a time domain Wiener deconvolution technique (e.g., Wu and Zeng, 1998; Ai *et al.*, 2005). A Gaussian parameter of 3 is applied here, roughly corresponding to a low-pass filter with a maximum frequency slightly greater than 1.0 Hz.

The strategy of stacking receiver functions should be noted here. Receiver functions from different backazimuths and epicentral distances are in general stacked to improve the single-to-noise ratio and suppress spurious arrival. However, synthetics show that the shape of both radial and tangential receiver functions varies greatly with backazimuth when a dipping interface exists (see Fig. 2). There is a potential hazard of choosing wrong stacking bounds (Cassidy, 1992). We thus take relatively tight stacking bounds for each station. The teleseismic events are divided into groups of backazimuth range less than 5°. Differences caused by epicentral distance also affect the waveforms, although not so strongly as backazimuth (Cassidy, 1992; Zhu *et al.*, 1995). Caution is taken to avoid a distance range span of more than 6°. Then the receiver functions in each backazimuth/epicentral distance group are stacked.

Figure 4 presents the 17 radial and tangential receiver functions after stacking, along with information on backazimuth for station JZ172. In each column, receiver functions are plotted at the same amplitude scale, so that we can observe the azimuthal amplitude variations clearly. Several prominent features can be seen in the radial and tangential receiver functions. The amplitude of tangential waveforms is large when be compared with the radial ones. The direct *P* wave shows negative polarity from backazimuths of about 114° to 217°, but it turns positive from 284° to 52°. The amplitude of the direct *P* wave is small on most receiver functions and the same for the *Ps* wave. There is a large secondary phase at about 1.8 sec after the direct *P* wave in both the radial and tangential components, and the large amplitude is consistently small at backazimuths where the polarity of the direct *P* phase changes in the tangential com-

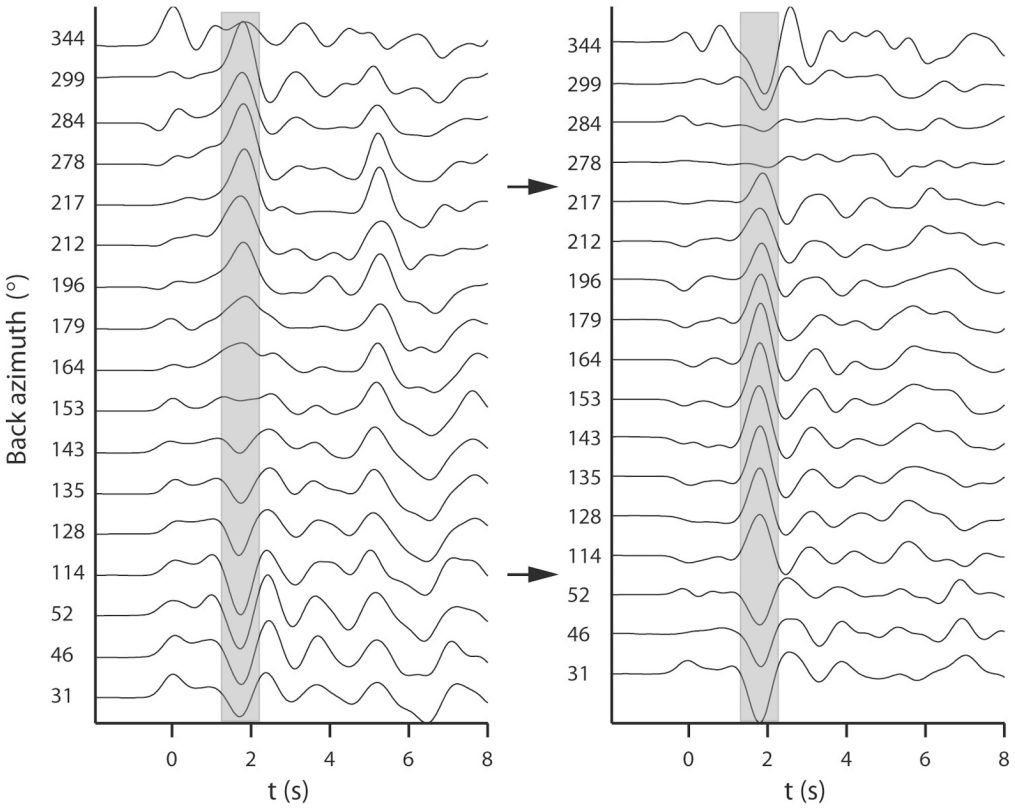

Figure 4. Receiver functions at station JZ172. Left and right panels are for radial and tangential components, respectively. Horizontal arrows point to where the polarity changes. Shadow zones indicate *PpPp* arrivals.

ponent. This simple amplitude and polarity pattern suggests that the dipping pattern of interfaces in the shallow structure are not complex. Because no large arrivals occurred before it, the large prominent phase following the direct *P* wave with changed polarity must be a *P*-type multiple *PpPp*, which reverberated in a shallow-dipping sedimentary layer.

To give an initial interpretation of our data, we first analyze the polarity changes observed on the tangential components. Figure 5 shows the dip direction constrained by polarity changes in the tangential receiver functions of each event for station JZ172. Using this simple criteria, we can constrain the dip direction to be between 254 and 292°.

A fast nonlinear simulated annealing algorithm (Ji *et al.*, 2002) is applied to determine the detailed structure under the station. The crustal model in the inversion consists of 18 planar-dipping interfaces, with layer thickness varying between 0.5 and 2.5 km. For simplification, Zhang and Langston (1992) used a constant Poisson's ratio of 0.25 to obtain the *P*-wave velocities in each inversion iteration. In the Bohai Bay Basin, this assumption is not appropriate for the well logging, and sonic data show that *S* velocity in the shallowest 1 km beneath the basin can be as low as 0.6 km/sec, resulting in a high V_p/V_s ratio (e.g., Zhao *et al.*, 2004). To further reduce the ill-posed problem of inversion, the strike direction and dip angle of the sedimentary layers are fixed in each forward calculation and based on the observations discussed earlier; all interfaces are assumed to have the same dip direction. The density in sedimentary layers is determined by the average relationship obtained from oil-drilling data in the Bohai Bay Basin (e.g., Zhao *et al.*, 2004), whereas for deeper layers, the density is calculated from the relationship $\rho = 0.32V_p + 0.77$ (Zhang and Langston, 1995).

Then the first 10 sec of the radial receiver functions are used to invert for the crustal velocity structure under station JZ172. The tangential receiver functions are not used because the tangential ones are very sensitive to the lateral heterogeneity. We search for the best-fit thicknesses, shear velocities, and V_p/V_s ratios. The ratio V_p/V_s is constrained between 1.73 and 2.73 for sedimentary layers, and *S* velocity in each sedimentary layer is allowed to change from 0.6 to 3.2 km/sec, an average velocity of the underlying crystalline basement rocks. Each time, we calculate the root-mean-square (rms) for the radial receiver function misfit and also compare waveforms of the tangential *P*-wave receiver functions. After each inversion, we change the dip angle and strike direction for the sedimentary layer between 5° and 15° and 164° and 202°, respectively, searching for the best-fit dipping parameters.

The best-fit model is shown in Figure 6b, with the shallow sedimentary layers striking 176° and dipping 12° to the west. Through numerous tests of the inversion and trial-and-error modeling, we find that if the dip angle of the following three deeper sedimentary layers is decreased to 5°, a much better waveform fit will be achieved. The sedimentary succession under this site is more than 6 km thick, and the Moho is at a depth of 27 km. The variation of Poisson's ratio with depth is also shown in this figure, changing from 2.7 near the surface to 1.74 at about 10 km in the upper crust. The synthetic radial receiver functions are presented in Figure 6a. The *PpPp*-amplitude comparison between the observed radial data and values predicted by the dipping model is give in Figure 6c. The consistency again confirms that the distinct phase with the largest amplitude following the *P* and *Ps* wave must be a *P*-type multiple-phase *PpPp*.

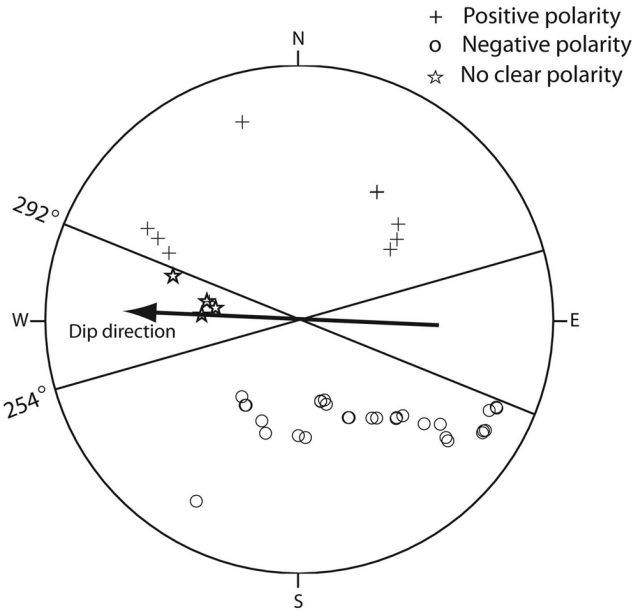

Figure 5. Polarities of tangential components versus backazimuth and distance. Pluses indicate positive polarity, circles indicate negative polarity, and small stars indicate events where no clear determination could be made. Distance increases radially outward, and backazimuth is positive clockwise from north.

The synthetic waveforms shown here seem to predict the main features of the observed receiver functions successfully, for example, the small amplitude of the direct *P* wave, the prominent *PpPp* multiple phase, and the *PmS* phase converted at Moho at about 5 sec. However, because of trade-offs among shallow and deeper layers, this model may not be accurate in all details, but suggests the main structural features under the complex Bohai Bay Basin.

Discussion and Conclusions

Despite the presence of dipping interfaces, anisotropy and scattering can also produce a nonzero tangential "*P*-wave" response. Considering the azimuthally consistent waveform pattern in both the radial and tangential data, however, the latter two cases can be ruled out as being major factors (Zhang and Langston, 1995).

A large time difference between the arrival time of radial and vertical waveforms for most backazimuths are observed while processing these data. This indicates that the radial direct *P* waveform can be severely distorted by shal-

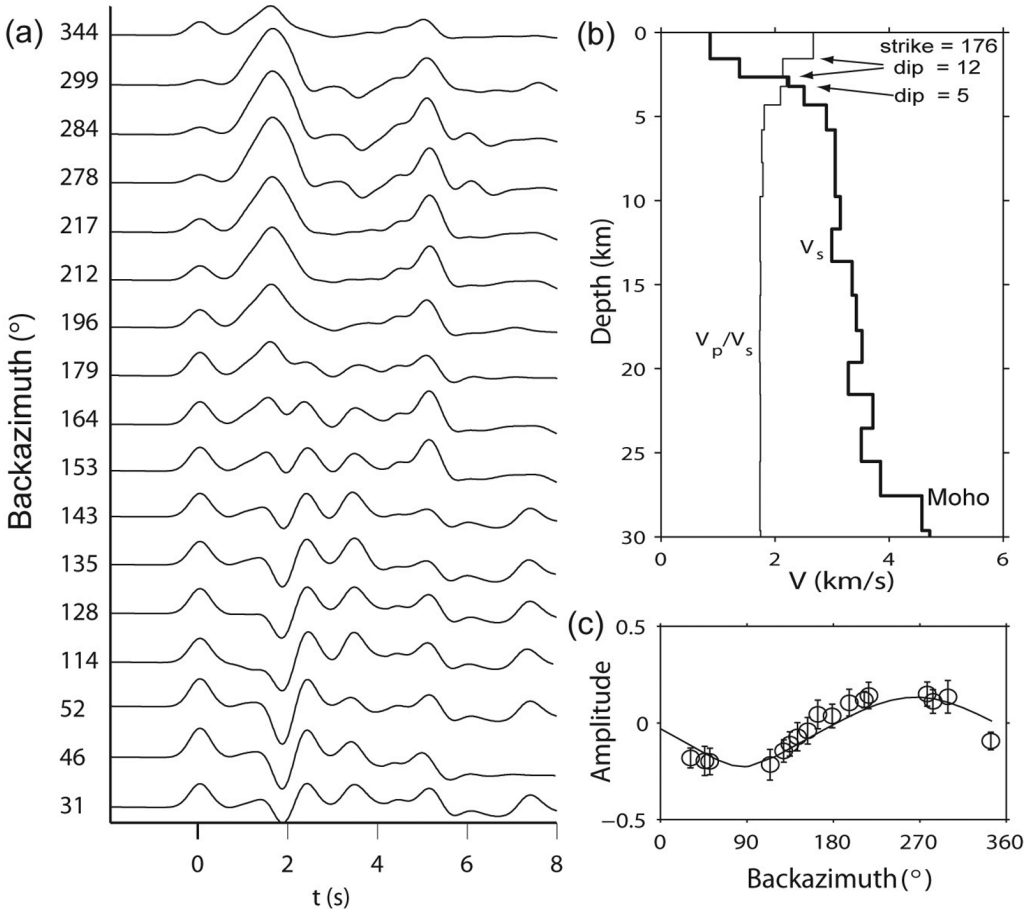

Figure 6. (a) Synthetic radial receiver functions for station JZ172. (b) Inverted shear velocity structure model (thick line) and variation of Poisson's ratio with depth (thin line). (c) Amplitudes of the observed *PpPp* phase (circles), reading errors (error bars), and theoretical prediction (solid line).

low structure, causing the delayed *Ps* phase, which converted at the shallow sedimentary interface, eventually emerging as the apparent "first arrival." This effect is severely sharpened by a shallow-dipping interface. So studies that usually use the radial component, like source studies, will introduce errors in derived source parameters if caution is not taken.

In the thick Cenozoic sedimentary layers in the Bohai Bay Basin, which are composed mainly of sandstones and organic-rich mudstones formed in lacustrine, transitional lacustrine/fluviatile, deltaic, or alluvial environments, the Poisson's ratio should not be regarded as a constant as was assumed in Zhang and Langston's work (1995). Jia and Zhang (2005) studied the crustal structure under different tectonic blocks in North China using deep seismic sounding (DSS) data, and found that the *P* velocity of the sediment cover in the Jizhong depression ranged from 1.5 to 5.2 km/sec; Zhao and Zheng (2005) observed that the travel-time residuals of *SH* waves recorded in the Bohai Bay Basin with respect to IASPEI91 model can be larger than 3.5 sec, especially for waves that travel through the Jizhong depression, which is in accordance with our inverted slow shear velocity and high V_p/V_s model in the shallower layers. The thick sedimentary layers and low-velocity distribution can also explain the delayed arrival time of the *PmS* phase converted at Moho with a depth of only 27 km.

The Jizhong depression, where station JZ172 is located, is one of many intracontinental basins developed during Cenozoic extensional tectonics of the North China plate and is characterized by north-northeast trending linear basement highs and lows bounded by normal faults (Zhao and Windley, 1990). The 176° strike direction of dipping interfaces obtained in this article, in general, is consistent with the north-northeast–south-southwest trend of surface geology in Jizhong depression. Figure 7 shows the geological interpretation of a cross section through the Jizhong depression, which is about 30 km to the north of station JZ172. The trend of west-dipping shallow layers can be clearly seen from the geological profile, which is well revealed by our result. The shallowest west-dipping layer corresponds to the sedimentary strata of Quaternary and Neogene age. This N + Q unconformity, a seismic marker, has also been rec-

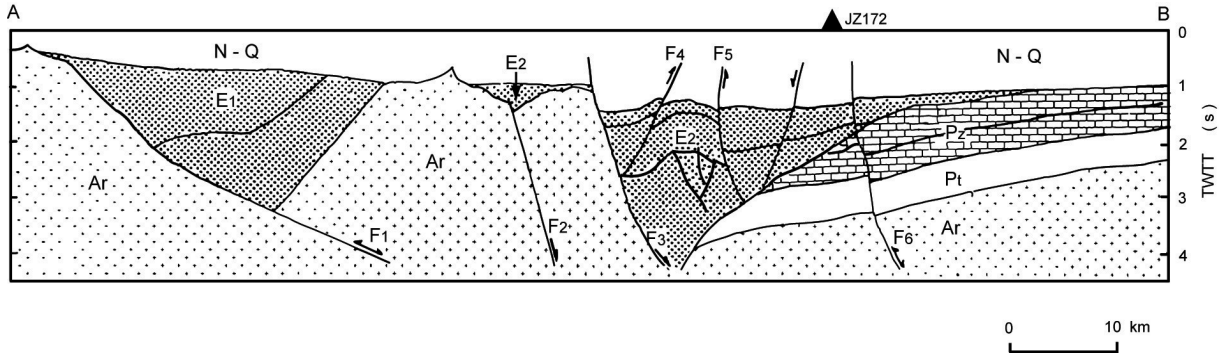

Figure 7. Geological interpretation along cross-section AB through the Jizhong depression (modified from Zhao and Windley, 1990). The seismic station JZ172 is projected onto the profile along the west–east direction. TWTT, two-way travel times; N, Neogene; Q, Quaternary; E1, Eocene; E2, Oligocene; Pz, Paleozoic; Pt, Proterozoic; Ar, Archean. The location of the section is shown in Figure 1.

ognized by drilling data (He and Zhu, 2001). The underlying layers may correspond to Paleogene and Pre-Tertiary strata, respectively. The Tertiary layer has the greatest thickness of about 5 km, forming a major reservoir for oil in this region.

Two distinctive Cenozoic structures, extensional and strike-slip structures, have been recognized throughout the Bohai Bay Basin (e.g., Lu *et al.*, 1997; Qi, 2004). We conclude from our results that extensional normal faults played an important role in the formation of dipping sedimentary layers. In fact, receiver functions of several other stations in the Bohai Bay Basin share the same features as that of station JZ172 (e.g., sites 161, 165, and 169 named in Zheng *et al.*, 2005), but with more limited backazimuth coverage. We noticed that all four stations are located near the boundary of half-grabens and horsts, where normal fault structures are well developed. It has also been reported that three episodes of extension took place between the Paleocene and Eocene, the Eocene and Oligocene, and the Oligocene and Miocene (Zhao and Windley, 1990). These extension episodes controlled by normal faults can be well illustrated by our inverted west-dipping sedimentary layers that are mainly composed of the Pre-Tertiary, Paleogene, and Neogene strata.

From these discussions, we can see that lateral heterogeneity of the shallow crustal structure modifies waveforms severely. With the help of prominent multiple waves, however, the teleseismic receiver functions can be applied independently to image the complex sedimentary structure in detail. The information inferred from the amplitude variation and polarity changes of multiples in both the radial and tangential components are very useful to constrain the sedimentary structure. By applying the teleseismic receiver function analysis to one station in the west edge of Bohai Bay Basin, we found west-dipping sedimentary layers with low velocity in the Jizhong depression, which may be caused by Tertiary extensional structures. For the Bohai Bay Basin, where shallow complexities are found, seismic recording must be analyzed with caution when utilized to study deeper structures.

Acknowledgments

We acknowledge the Broadband Seismic Array Laboratory, Institute of Geology and Geophysics, Chinese Academy of Sciences for providing the digital seismic data. We thank Zheng Tianyu for useful discussion. An anonymous reviewer provided constructive suggestions that greatly improved the manuscript. This work is supported by the National Science Foundation of China (grant nos. 40404004 and 40404003).

References

Ai, Y., D. Zhao, X. Gao, and W. Xu (2005). The crust and upper mantle discontinuity structure beneath Alaska inferred from receiver functions, *Phys. Earth. Planet. Interiors* **150,** 339–350.

Allen, M. B., D.I.M. Macdonald, X. Zhao, S. J. Vincent, and C. Brouet-Menzies (1997). Early Cenozoic two-phase extension and late Cenzoic thermal subsidence and inversion of the Bohai Basin, *Mar. Pet. Geol.* **14,** 951–972.

Ammon, C. J., G. E. Randall, and G. Zandt (1990). On the nonuniqueness of receiver function inversions, *J. Geophys. Res.* **95,** 15,303–15,318.

Anandakrishnan, S., and J. P. Winberry (2004). Antarctic subglacial sedimentary layer thickness from receiver function analysis, *Global Planet. Change* **42,** 167–176.

Burdick, L. J., and C. A. Langston (1977). Modeling crustal-structure through the used of converted phases in teleseismic body-waveforms. *Bull. Seism. Soc. Am.* **67,** 677–691.

Cassidy, J. F. (1992). Numerical experiments in broadband receiver function analysis, *Bull. Seism. Soc. Am.* **82,** no. 3, 1453–1474.

He, S., W. Zhu, and L. Li (2001). Sedimentary evolution and Neogene reservoir-seal assemblage analysis of Bozhong depression, *Acta Pet. Sin.* **22,** no. 2, 38–43 (in Chinese).

Ji, C., D. J. Wald, and D. V. Helmberger (2002). Source description of the 1999 Hector Mine, California, Earthquake, Part I: Wavelet domain inversion theory and resolution analysis, *Bull. Seism. Soc. Am.* **92,** 1192–1207.

Jia, S. X., and X. K. Zhang (2005). Crustal structure and comparison of different tectonic blocks in North China, *Chin. J. Geophys.* **48,** no. 3, 611–620 (in Chinese).

Langston, C. A. (1977). The effect of planar dipping structure on source and receiver responses for constant ray parameter, *Bull. Seism. Soc. Am.* **67,** no. 4, 1029–1050.

Li, P. L. (2004). Oil/gas distribution patterns in Dongying depression, Bohai Bay Basin, *J. Pet. Sci. Eng.* **41,** 57–66.

Lu, K. Z., J. F. Qi, and J. S. Dai (1997). *Tectonic Model of Cenozoic*

Petroliferous Basin Bohai Bay Province, Geological Publishing House, Beijing (in Chinese).

Owens, T. H., and R. S. Crosson (1988). Shallow structure effects on broadband teleseismic P waveforms, *Bull. Seism. Soc. Am.* **78,** no. 1, 96–108.

Qi, J. F. (2004). Two tectonic systems in the Cenozoic Bohai Bay Basin and their genetic interpretation, *Geol. China* **31,** no. 1, 15–22 (in Chinese).

Ren, J. Y., K. Tamaki, S. T. Li, and J. X. Zhang (2002). Late Mesozoic and Cenozoic rifting and its dynamic setting in Eastern China and adjacent areas, *Tectonophysics* **344,** 175–205.

Wu, Q. J., and R. S. Zeng (1998). The crustal structure of Qinghai-Xizang plateau inferred from broadband teleseismic waveform, *Chin. J. Geophys.* **41,** 669–679 (in Chinese).

Yang, Y., and T. Xu (2004). Hydrocarbon habitat of the offshore Bohai Basin, *Mar. Pet. Geol.* **21,** 691–708.

Ye, H., K. M. Shedlock, S. J. Hellinger, and J. C. Sclater (1985). The North China basin: an example of a Cenozoic rifted intraplate basin, *Tectonics* **4,** 153–169.

Zhang, J., and C. A. Langston (1995). Dipping structure under Dourbes, Belgium, determined by receiver function modeling and inversion, *Bull. Seism. Soc. Am.* **85,** no. 1, 254–268.

Zhao, L., T. Y. Zheng, and W. W. Xu (2004). Modeling the Jiyang depression, Northern China, using a wave-field extrapolation finite-difference method and waveform inversion, *Bull. Seism. Soc. Am.* **94,** no. 3, 988–1001.

Zhao, L., and T. Y. Zheng (2005). Seismic structure of the Bohai Bay Basin, northern China: implications for basin evolution, *Earth. Planet. Sci. Lett.* **231,** 9–22, doi 10.1016/j.epsl.2004.12.028.

Zhao, L. F., W. M. Wang, J. Li, and Z. X. Yao (2006). Modelling the seismic response of basin-edge structure by a sequential waveform method, *Tectonophysics* **420,** 493–507.

Zhao, Z. Y., and B. F. Windley (1990). Cenozoic tectonic extension and inversion of the Jizhong Basin, Hebei, northern China, *Tectonophysics* **185,** 83–89.

Zheng, T. Y., L. Zhao, and L. Chen (2005). A detailed receiver function image of the sedimentary structure in the Bohai Bay Basin, *Phys. Earth. Planet. Interiors* **152,** 129–143.

Zhu, L. P., and H. Kanamori (2000). Moho depth variation in southern California from teleseismic receiver functions, *J. Geophys. Res.* **105,** no. B2, 2069–2980.

Zhu, L. P., T. J. Owens, and G. E. Randall (1995). Lateral variation in crustal structure of the Northern Tibetan plateau inferred from teleseismic receiver functions, *Bull. Seism. Soc. Am.* **85,** no. 6, 1531–1540.

Institute of Geology and Geophysics
Chinese Academy of Sciences
State Key Laboratory of Lithosphere Evolution
100029, Beijing, China
juanli@mail.iggcas.ac.cn

Manuscript received 18 July 2006.